Observation of seasonal variation of atmospheric multiple-muon events in the NOvA Near Detector

M. A. Acero *et al.* (NOvA Collaboration)

Phys. Rev. D **99**, 122004 — Published 28 June 2019

DOI: 10.1103/PhysRevD.99.122004

FERMILAB-PUB-19-179-ND

Observation of seasonal variation of atmospheric multiple-muon events in the NOvA Near Detector

M. A. Acero,[2] P. Adamson,[12] L. Aliaga,[12] T. Alion,[39] V. Allakhverdian,[27] S. Altakarli,[46] N. Anfimov,[27] A. Antoshkin,[27,31] A. Aurisano,[6] A. Back,[24] C. Backhouse,[44] M. Baird,[19,39,45] N. Balashov,[27] P. Baldi,[25] B. A. Bambah,[17] S. Bashar,[43] K. Bays,[4,21] S. Bending,[44] R. Bernstein,[12] V. Bhatnagar,[32] B. Bhuyan,[14] J. Bian,[25,31] J. Blair,[16] A.C. Booth,[39] P. Bour,[9] C. Bromberg,[29] N. Buchanan,[8] A. Butkevich,[22] S. Calvez,[8] M. Campbell,[44] T. J. Carroll,[42] E. Catano-Mur,[24,47] A. Cedeno,[46] S. Childress,[12] B. C. Choudhary,[11] B. Chowdhury,[35] T. E. Coan,[37] M. Colo,[47] L. Corwin,[36] L. Cremonesi,[44] G. S. Davies,[19] P. F. Derwent,[12] P. Ding,[12] Z. Djurcic,[1] D. Doyle,[8] E. C. Dukes,[45] H. Duyang,[35] S. Edayath,[7] R. Ehrlich,[45] G. J. Feldman,[15] P. Filip,[23] W. Flanagan,[10] M. J. Frank,[34,45] H. R. Gallagher,[43] R. Gandrajula,[29] F. Gao,[33] S. Germani,[44] A. Giri,[18] R. A. Gomes,[13] M. C. Goodman,[1] V. Grichine,[28] M. Groh,[19] R. Group,[45] B. Guo,[35] A. Habig,[30] F. Hakl,[20] J. Hartnell,[39] R. Hatcher,[12] A. Hatzikoutelis,[41] K. Heller,[31] J. Hewes,[6] A. Himmel,[12] A. Holin,[44] B. Howard,[19] J. Huang,[42] J. Hylen,[12] F. Jediny,[9] C. Johnson,[8] M. Judah,[8] I. Kakorin,[27] D. Kalra,[32] D.M. Kaplan,[21] R. Keloth,[7] O. Klimov,[27] L.W. Koerner,[16] L. Kolupaeva,[27] S. Kotelnikov,[28] A. Kreymer,[12] Ch. Kulenberg,[27] A. Kumar,[32] C. D. Kuruppu,[35] V. Kus,[9] T. Lackey,[19] K. Lang,[42] S. Lin,[8] M. Lokajicek,[23] J. Lozier,[4] S. Luchuk,[22] S. Magill,[1] W. A. Mann,[43] M. L. Marshak,[31] V. Matveev,[22] D. P. Méndez,[39] M. D. Messier,[19] H. Meyer,[46] T. Miao,[12] W. H. Miller,[31] S. R. Mishra,[35] A. Mislivec,[31] R. Mohanta,[17] A. Moren,[30] L. Mualem,[4] M. Muether,[46] S. Mufson,[19] K. Mulder,[44] R. Murphy,[19] J. Musser,[19] D. Naples,[33] N. Nayak,[25] J. K. Nelson,[47] R. Nichol,[44] G. Nikseresht,[21] E. Niner,[12] A. Norman,[12] T. Nosek,[5] A. Olshevskiy,[27] T. Olson,[43] J. Paley,[12] R. B. Patterson,[4] G. Pawloski,[31] O. Petrova,[27] R. Petti,[35] D. D. Phan,[42] R. K. Plunkett,[12] B. Potukuchi,[26] C. Principato,[45] F. Psihas,[19] V. Raj,[4] R. A. Rameika,[12] B. Rebel,[12,48] P. Rojas,[8] V. Ryabov,[28] O. Samoylov,[27] M. C. Sanchez,[24] P. Schreiner,[1] I. S. Seong,[25] P. Shanahan,[12] A. Sheshukov,[27] P. Singh,[11] V. Singh,[3] E. Smith,[19] J. Smolik,[9] P. Snopok,[21] N. Solomey,[46] E. Song,[45] A. Sousa,[6] K. Soustruznik,[5] M. Strait,[31] L. Suter,[12] A. Sutton,[45] R. L. Talaga,[1] P. Tas,[5] R. B. Thayyullathil,[7] J. Thomas,[44,48] E. Tiras,[24] S. C. Tognini,[13] D. Torbunov,[31] J. Tripathi,[32] A. Tsaris,[12] Y. Torun,[21] J. Urheim,[19] P. Vahle,[47] J. Vasel,[19] L. Vinton,[39] P. Vokac,[9] T. Vrba,[9] M. Wallbank,[6] B. Wang,[37] T. K. Warburton,[24] M. Wetstein,[24] M. While,[36] D. Whittington,[40,19] S. G. Wojcicki,[38] J. Wolcott,[43] N. Yadav,[14] A. Yallappa Dombara,[40] K. Yonehara,[12] S. Yu,[1,21] S. Zadorozhnyy,[22] J. Zalesak,[23] and R. Zwaska[12]

(The NOvA Collaboration)

[1] *Argonne National Laboratory, Argonne, Illinois 60439, USA*
[2] *Universidad del Atlantico, Km. 7 antigua via a Puerto Colombia, Barranquilla, Colombia*
[3] *Department of Physics, Institute of Science, Banaras Hindu University, Varanasi, 221 005, India*
[4] *California Institute of Technology, Pasadena, California 91125, USA*
[5] *Charles University, Faculty of Mathematics and Physics, Institute of Particle and Nuclear Physics, Prague, Czech Republic*
[6] *Department of Physics, University of Cincinnati, Cincinnati, Ohio 45221, USA*
[7] *Department of Physics, Cochin University of Science and Technology, Kochi 682 022, India*
[8] *Department of Physics, Colorado State University, Fort Collins, CO 80523-1875, USA*
[9] *Czech Technical University in Prague, Brehova 7, 115 19 Prague 1, Czech Republic*
[10] *University of Dallas, 1845 E Northgate Drive, Irving, Texas 75062 USA*
[11] *Department of Physics and Astrophysics, University of Delhi, Delhi 110007, India*
[12] *Fermi National Accelerator Laboratory, Batavia, Illinois 60510, USA*
[13] *Instituto de Física, Universidade Federal de Goiás, Goiânia, Goiás, 74690-900, Brazil*
[14] *Department of Physics, IIT Guwahati, Guwahati, 781 039, India*
[15] *Department of Physics, Harvard University, Cambridge, Massachusetts 02138, USA*
[16] *Department of Physics, University of Houston, Houston, Texas 77204, USA*
[17] *School of Physics, University of Hyderabad, Hyderabad, 500 046, India*
[18] *Department of Physics, IIT Hyderabad, Hyderabad, 502 205, India*
[19] *Indiana University, Bloomington, Indiana 47405, USA*
[20] *Institute of Computer Science, The Czech Academy of Sciences, 182 07 Prague, Czech Republic*
[21] *Department of Physics, Illinois Institute of Technology, Chicago IL 60616, USA*
[22] *Inst. for Nuclear Research of Russia, Academy of Sciences 7a, 60th October Anniversary prospect, Moscow 117312, Russia*
[23] *Institute of Physics, The Czech Academy of Sciences, 182 21 Prague, Czech Republic*
[24] *Department of Physics and Astronomy, Iowa State University, Ames, Iowa 50011, USA*
[25] *Department of Physics and Astronomy, University of California at Irvine, Irvine, California 92697, USA*
[26] *Department of Physics and Electronics, University of Jammu, Jammu Tawi, 180 006, Jammu and Kashmir, India*
[27] *Joint Institute for Nuclear Research, Dubna, Moscow region 141980, Russia*
[28] *Nuclear Physics and Astrophysics Division, Lebedev Physical Institute, Leninsky Prospect 53, 119991 Moscow, Russia*
[29] *Department of Physics and Astronomy, Michigan State University, East Lansing, Michigan 48824, USA*

[30]Department of Physics and Astronomy, University of Minnesota Duluth, Duluth, Minnesota 55812, USA
[31]School of Physics and Astronomy, University of Minnesota Twin Cities, Minneapolis, Minnesota 55455, USA
[32]Department of Physics, Panjab University, Chandigarh, 160 014, India
[33]Department of Physics, University of Pittsburgh, Pittsburgh, Pennsylvania 15260, USA
[34]Department of Physics, University of South Alabama, Mobile, Alabama 36688, USA
[35]Department of Physics and Astronomy, University of South Carolina, Columbia, South Carolina 29208, USA
[36]South Dakota School of Mines and Technology, Rapid City, South Dakota 57701, USA
[37]Department of Physics, Southern Methodist University, Dallas, Texas 75275, USA
[38]Department of Physics, Stanford University, Stanford, California 94305, USA
[39]Department of Physics and Astronomy, University of Sussex, Falmer, Brighton BN1 9QH, United Kingdom
[40]Department of Physics, Syracuse University, Syracuse NY 13210, USA
[41]Department of Physics and Astronomy, University of Tennessee, Knoxville, Tennessee 37996, USA
[42]Department of Physics, University of Texas at Austin, Austin, Texas 78712, USA
[43]Department of Physics and Astronomy, Tufts University, Medford, Massachusetts 02155, USA
[44]Physics and Astronomy Dept., University College London, Gower Street, London WC1E 6BT, United Kingdom
[45]Department of Physics, University of Virginia, Charlottesville, Virginia 22904, USA
[46]Department of Mathematics, Statistics, and Physics, Wichita State University, Wichita, Kansas 67206, USA
[47]Department of Physics, College of William & Mary, Williamsburg, Virginia 23187, USA
[48]Department of Physics, University of Wisconsin-Madison, Madison, Wisconsin 53706, USA

Using two years of data from the NOvA Near Detector at Fermilab, we report a seasonal variation of cosmic ray induced multiple-muon ($N_\mu \geq 2$) event rates which has an opposite phase to the seasonal variation in the atmospheric temperature. The strength of the seasonal multiple-muon variation is shown to increase as a function of the muon multiplicity. However, no significant dependence of the strength of the seasonal variation of the multiple-muon variation is seen as a function of the muon zenith angle, or the spatial or angular separation between the correlated muons.

PACS numbers:

I. INTRODUCTION

This paper presents new measurements of the seasonality of underground multiple muons ($N_\mu \geq 2$) produced from cosmic ray showers in the atmosphere. Incoming cosmic ray nuclei interacting with the upper atmosphere produce a flux of pions (π), kaons (K), and other mesons at an altitude directly dependent upon the upper atmosphere density profile. These mesons either interact with the atmosphere to produce a hadronic cascade that contains additional mesons, or they decay to final states with muonic content. The relative probability of each primary and secondary meson decaying, or having a strong interaction with the atmosphere, depends on its energy and the density of the atmosphere near its production point. The density of the atmosphere depends upon many factors, with local temperature being the dominant one. The mean temperature of the upper atmosphere varies during the seasons, so the corresponding high energy cosmic muon rate is expected to vary. The high energy muon flux increases during the summer months due to the decrease in the density of the upper atmosphere, which increases the probability that a meson will directly decay into a muon instead of having a secondary strong interaction. Numerous underground detectors [1–15] at a variety of underground depths have measured this expected seasonal variation via the flux of single-muon events.

The atmospheric particle showers produced by the interactions of cosmic ray nuclei produce muons of varying energies. The overburden associated with each underground detector will determine the minimum energy muon that can be observed. The highest energy muons usually come from π's and K's produced in the first interaction of the primary cosmic ray in the atmosphere. The predominance of muons arising from daughters of the primary interaction is a consequence of the steeply falling power law for the cosmic ray energy spectrum $\propto E^{-2.7}$, combined with Feynman scaling [16] for the leading hadron in the primary interaction. Observed underground single-muon events are produced by atmospheric showers in which the other muons, associated with the hadronic cascade, have either ranged out prior to reaching the detector or missed the detector due to the shower's angular divergence and extent at the detector location. Thus it is expected that the observed muon in most single-muon events is the highest energy muon in the shower. Multiple-muon events in an underground detector require one or more additional high energy muons at a small enough transverse distance to be observed in the spatial limits of the detector.

One important consideration in studying temperature effects in the atmosphere is the value of the critical energies for the π and K. The critical energy is defined as the energy for which the π (K) interaction probability and decay probability are equal. Above the critical energy, more mesons interact before they decay. Below the critical energy, more mesons decay before they interact. The value for the π (K) is 135 GeV (850 GeV). Most muons seen in shallow detectors (minimum energy at the Earth's surface $\left(E_\mu^{surface}\right) < 100\,\text{GeV}$) are from the decay of mesons below their critical energies, which reduces the effect of temperature and density fluctuations caused by seasonal effects, compared to higher energies measured in deeper detectors.

The MINOS Near and Far Detectors observed a different seasonal variation for multiple-muon events than for single muons [17]. The multiple-muon rate was observed to unexpectedly increase during the winter months in the shallow underground Near Detector ($E_\mu^{surface} > 54\,\mathrm{GeV}$), In the deeper Far Detector ($E_\mu^{surface} > 730\,\mathrm{GeV}$), the seasonal variation depended upon the spatial separation of the muons in the event, e.g. a winter maximum was seen for events with muons within 4.5 m and a summer maximum for events with muons separated more than 8 m.

At low energy ($E_\mu^{surface} \approx 1\,\mathrm{GeV}$), muon decay plays a role in seasonal effects. We note that muon detectors located near the surface, such as the GRAPES experiment ($E_\mu^{surface} > 1\,\mathrm{GeV}$), measured a winter maximum for their muon rate [18]. The DECOR experiment ($E_\mu^{surface} > 2\,\mathrm{GeV}$), also measured a winter maximum for multiple muons on the surface [19]. DECOR attributed their result to geometric effects arising from altitude differences, but MINOS showed that at a depth of 225 meters water equivalent (mwe), the altitude differences were too small to explain the effect [17].

The goal of this analysis of NOvA data is to confirm and to further investigate the seasonal effect that was measured in the MINOS experiment for multiple muons [17], with larger statistics, a simpler detector geometry, and looking at the effect as a function of more observables. This paper presents the multiple-muon rate observed in the NOvA Near Detector (ND) at Fermilab at a depth of 225 mwe. The NOvA ND is at the same depth as the MINOS Near Detector but uses a different detector design. The muon rate in NOvA is measured using data from 8 April 2015 to 16 April 2017, representing two complete calendar years of exposure. This period does not coincide with the data presented by MINOS. The strength of the multiple-muon seasonal rate variation is studied using a Rayleigh power analysis, by looking for correlations with the effective atmospheric temperature, and by fitting the rate to a cosine function. The multiple-muon seasonal rate in NOvA is measured as a function of muon multiplicity and as a function of several geometric variables.

II. THE NOVA NEAR DETECTOR AND MUON AND TEMPERATURE DATA

The NOvA ND is located underground at a depth of 94 m [20]. It was primarily designed to study neutrinos produced by the Fermilab NuMI beam [21]. The detector is a segmented tracking calorimeter which is constructed from planes of extruded polyvinyl chloride (PVC) cells [22]. Each NOvA cell has a width of 3.8 cm, a depth of 5.9 cm, and is 3.9 m long. The cells are filled with liquid scintillator [23] and the signal scintillation light is collected and transported to the readout by wavelength-shifting fiber which runs the length of each cell. The light collected by the fibers is routed to avalanche photodiodes (APD) and digitized. Light producing a signal in the APD above a set threshold is recorded as a hit. The detector and electronics are located in a climate controlled environment which reduces one source of seasonal influence.

The detector consists of two parts: a fully active region and a muon ranger. The active region contains 192 planes of cells. Each plane is 3.9 m by 3.9 m in cross section. The orientation of the planes alternates between vertical and horizontal views around the beam to allow 3D reconstruction. The 192 planes cover a longitudinal distance along the NuMI beam of 12.75 m. The muon ranger is located at the downstream end in the beam direction. It consists of 22 scintillator planes of size 3.9 m horizontally by 2.7 m vertically. The muon ranger is 2.85 m long. There are 10 steel planes of thickness 10 cm each interleaved with a pair of scintillator planes. Together, the complete detector has 20,192 cells within the 214 planes. The area at the top of the detector is $50\,\mathrm{m}^2$ in the active detector and $11\,\mathrm{m}^2$ in the muon ranger.

Cosmic rays are recorded in the NOvA ND with an activity trigger which requires at least 10 hits on at least 8 planes in total with at least 3 planes hit in each of the two views. In addition, there must be at least 5 planes with hits in a window of 6 sequential planes. The typical activity trigger rate is 39 triggers/s. Each trigger causes a readout of 50 or 100 μs of data which fully encompasses the hits which satisfy the triggering condition. This hit data has a single hit timing resolution of 5-10 ns. In this analysis, tracks registering in the detector with temporal separation of less than 100 ns are considered to be correlated and part of a multiple-muon event. Data overlapping with the NuMI beam spill was not used for this analysis. Cosmic muon reconstruction is performed using a Hough Transform [24] which finds hits that line up in each view. The two views are then matched to produce a 3D reconstructed track.

In order to reduce the number of misreconstructed events to a negligible level, additional analysis selection criteria were applied to the events. NOvA monitors the quality of its data continuously and only those data meeting publication quality standards were used in this analysis. Reconstructed track directions along the planes of the detector were discarded because many resulted from bad matching of 2D tracks. This was done by selecting the direction cosines in the X and Z directions; $|\cos\theta_z| \geq 0.02$ and $\cos\theta_x \geq 0.02$ or $\cos\theta_x \leq 0$. In addition, to remove short tracks consistent with electrons from bremsstrahlung above the detector, we impose a throughgoing requirement by demanding the first and last hit on all tracks be within 50 cm of the detector edges. This selection removes stopping muons which are the 2% of incoming muons with the lowest energies.

Using a Monte Carlo simulation (MC) based on the CRY simulation [25], the reconstruction efficiency after all selection criteria was 69%. This was consistent with the result that 73% of all activity triggers gave at least one selected muon. The inefficiency comes from both the 10-hit requirement and reconstruction difficulties for steep tracks. The efficiency estimate is not important for the rest of the analysis since it does not depend on time during the year. A two-muon simulation was developed using the single-muon simulation and randomly placing a second parallel muon in the detector. Both muons were reconstructed and passed the analysis criteria with an efficiency of 37%. The two-muon efficiency was reduced some due to confusion when 2D tracks overlapped in one view. A visual inspection of several thousand triggers showed the impurity from triggers not containing muons (before reconstruction) to be below 1%. There was agreement of the distributions of track positions and angles between the data and simulation [26]. Other than as a check on the validity of the reconstruction, a simulation was not used in the analysis presented here.

The reconstructed track multiplicity for multiple-muon events in NOvA is shown in Fig. 1. The maximum reconstructed multiplicity event found in our sample is 10 muons. In this paper, the multiplicity always refers to the observed multiplicity. We do not correct for muons within air showers that reach the depth of the detector but miss it laterally. Thus the muon multiplicity is a detector (acceptance) dependent quantity.

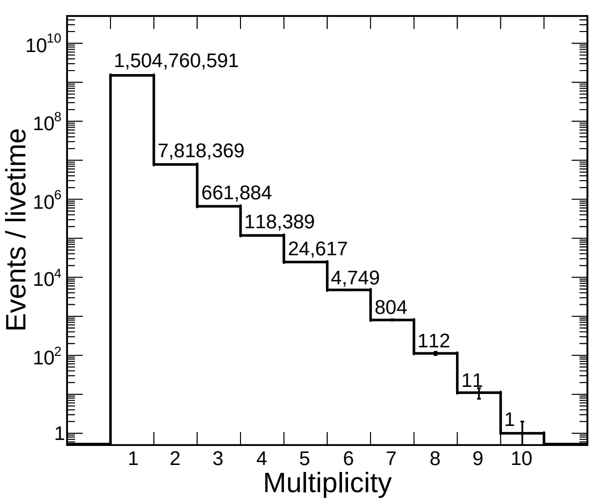

FIG. 1: Observed multiplicity distribution for single- and multiple-muon events in the NOvA ND. The livetime for this exposure was 55.29×10^6 s. Note that the vertical axis in the figure is shown on a logarithmic scale.

The total elapsed time for this period is 63.85×10^6 s. Event rates were calculated during periods in which data was recorded that were up to an hour long. Rates during longer periods were calculated using the number of observed events and the corresponding livetime. The total detector livetime was 55.29×10^6 s representing a livetime fraction of 86%. The livetime was not uniformly distributed, but there was ample statistics to calculate a rate during every month. The time between multiple-muon events during periods of livetime is shown in Fig. 2. The distribution drops according to a power law over several orders of magnitude, as expected for random uncorrelated events.

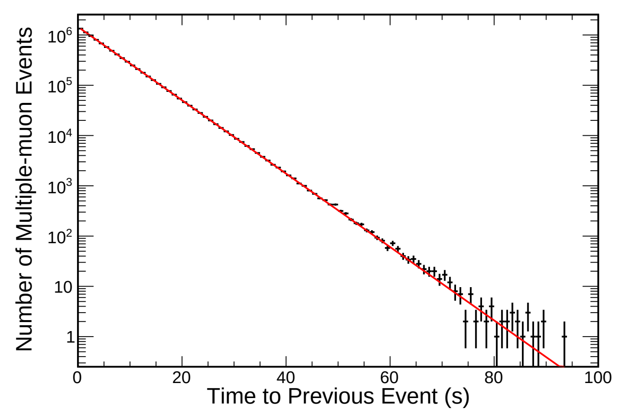

FIG. 2: Time between multiple-muon events in the NOvA ND. An exponential fit is shown, as expected for random events with no correlations. The mean rate from this fit is 0.17 s^{-1}.

Atmospheric temperature data is provided four times per day by the European Center for Medium-Range Weather Forecast (ECMWF) at 37 pressure levels, ranging from 1 hPa to 1,000 hPa, corresponding to altitudes up to 50 km [27]. ECMWF provides interpolated temperature values on the corners of a grid, whose latitude and longitude values range from (41.25° N, 87.75° W) to (42.00° N, 88.50° W) with a 0.75° increment in each direction. This area well matches the production site for most of the muons reaching the NOvA ND at 41.50° N, 88.16° W [26, 28]. These temperature values are used to construct $T_{\rm eff}$, which is their average weighted over the altitude for single-muon production [29].

III. SEASONAL ANALYSIS

The observed rate of multiple muons (R_μ) is shown using bins corresponding to one month in time in Fig. 3. A clear seasonal variation is observed. The size of the winter/summer rate change differs between the two years of data. A number of consistency checks showed that there was no difference in detector performance affecting this analysis during those two years [26]. The effective temperature calculated at the production altitude for single muons above the NOvA ND was calculated in a similar way as in reference [17]. The monthly values of $\Delta(T_{\rm eff})/\langle T_{\rm eff}\rangle$ and $\Delta(R_\mu)/\langle R_\mu\rangle$ are shown in Fig. 4. An anticorrelation between these two quantities is evident.

Since the frequency we were testing is well known, a frequency analysis using the Lomb-Scargle method [30] was performed on the multiple-muon data as a consistency check. The highest power was found at a frequency corresponding to a year [26]. A strong seasonal effect is apparent in Fig. 3. To further study this variation as a function of several observables, it was necessary to select an *a priori* way to quantify the sign and strength of the effect. We chose three complementary methods: 1) a Rayleigh power analysis, 2) the correlation coefficient α_T of the rate with effective temperature, and 3) comparison of the rate change to a cosine function. MINOS has shown a seasonal multiple-muon effect with an opposite phase to that for the single muons [17], however we extended the previous qualitative analysis with these methods. Each method has some advantages and disadvantages in this context.

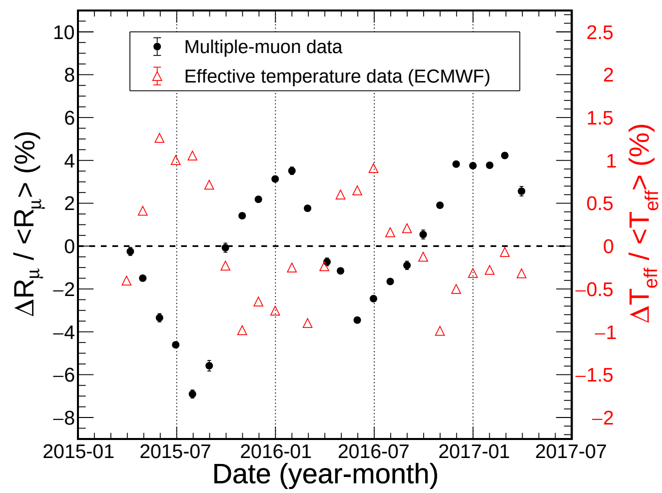

FIG. 4: Rate variation of the multiple muons as a function of month shown with the variation in the effective atmospheric temperature for single muons above the NOvA ND. The mean values are $\langle R_\mu \rangle = 0.168\ s^{-1}$ and $\langle T_{\rm eff} \rangle = 222$ K.

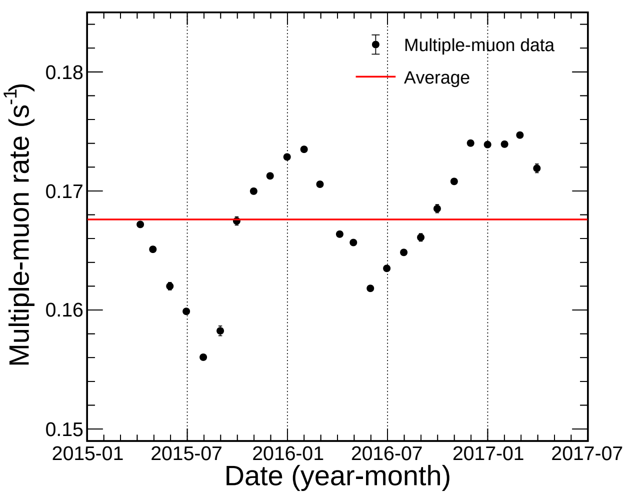

FIG. 3: Rate of multiple muons in the NOvA ND as a function of month and year.

A. Rayleigh analysis

The Rayleigh analysis uses the binned Rayleigh power (P_R), which is defined as:

$$P_R = \frac{\left\{\sum_{i=1}^{n} x_i \sin(\omega t_i)\right\}^2 + \left\{\sum_{i=1}^{n} x_i \cos(\omega t_i)\right\}^2}{N}, \quad (1)$$

where N is the total number of events, n is the number of bins, $x_i \equiv x(t_i)$ is the number of events in each bin, $\omega = 2\pi/(1 \text{ year})$ is the angular frequency, and t_i is the time of the center of each bin. The Rayleigh power can be thought of as the deviation from the origin for a random walk of N steps. Since the frequency is known, it gives an absolute probability that unseasonal data would give the observed power. This method is compromised by gaps in the data for small bin sizes, but for monthly or even weekly bins there are no gaps. However, to compare the size of the power for subsamples of the data, the number of events in each subsample needs to be identical. It is not useful, for example, for comparing the power of different multiplicities because the sample sizes widely differ. The binning in time is chosen to have a negligible effect on the calculation of P_R. The chance probability that the obtained value of the Rayleigh power does not come from a random flat distribution is $1 - e^{-P_R}$. All probabilities obtained in this analysis are near unity, but the value of P_R itself is used to see if there are trends as a function of interesting variables.

A calculation of the Rayleigh power using the data in Fig. 3 gives a value $P_R = 3665$. The probability that this is the result of non-seasonal random data is e^{-3665}, which is negligible.

B. Correlation coefficient

Seasonal variations for single muons have been studied with a correlation coefficient α_T defined by [29]

$$\frac{\Delta R_\mu}{\langle R_\mu \rangle} = \alpha_T \frac{\Delta T_{\rm eff}}{\langle T_{\rm eff} \rangle}, \quad (2)$$

where $\langle R_\mu \rangle$ is the mean muon event rate for the complete observation period, and corresponds to the rate for an effective atmospheric temperature equal to $\langle T_{\rm eff} \rangle$. The magnitude of the temperature coefficient α_T is dependent on the muon energy at production and hence the depth of the detector. The effective temperature $T_{\rm eff}$ is a weighted average of temperature measurements over the region of the atmosphere where muons originate [29]. The value of $T_{\rm eff}$ tracks the actual temperatures at 37 altitudes calculated on a 6-hour basis. This temperature is correlated with the density of the atmosphere and hence the competition between interaction and decay for π's and K's as they traverse the varying density atmosphere. As a consequence of the steeply falling energy distribution of cosmic ray primaries, only considering hadrons in the first interaction is a good approximation for single muons. A theoretical formula for α_T for single muons derived in reference [29] gives a value that is always positive.

For this multiple-muon analysis, a limitation is that $T_{\rm eff}$ in Eq. 2 has been calculated by weighting the vertical temperature distribution with the interaction length of the primary cosmic ray together with the lifetime of a secondary hadron produced in the first interaction [30]. However, the seasonal behavior of the rate for multiple-muon events is not expected to be precisely represented by a simple formula due to the many competing effects such as non-leading mesons from the first interaction, and mesons from secondary interactions, etc. Multiple muons observed underground may predominantly result from hadrons produced in secondary interactions or those further into a hadronic shower. The calculation of $T_{\rm eff}$ used above is a poorer approximation in the determination of α_T than for single muons. However, the gradient of temperature variations in the atmosphere is fairly smooth in both winter and summer, so $T_{\rm eff}$ may be useful in tracking the multiple-muon effective temperature variation as a function of date and is used in the analysis below. Using the data in Fig. 4, we find α_T = -4.14 $\pm$ 0.07. The quoted uncertainty comes from the fit and does not include the systematic uncertainties discussed below.

C. Cosine fit

Our third measure of the strength of the seasonal variation is the amplitude of a fit of the data to a cosine function. The fitting function used is

$$f(t) = V_0 + V\cos(\omega t + \phi), \tag{3}$$

and the amplitudes V are compared in the next section. While temperatures are predictably warmer in the summer and colder in the winter, the variation does not typically follow a cosine function, so any fit will necessarily be poorly described by that function. In fact the difference between the two years in Fig. 3 is larger than the differences seen in reference [13]. Nevertheless, we find such a fit to be a useful way to parametrize some of the data. The fits were performed on the data binned according to the month of the year in which the data were recorded.

Averaging over the two years of NOvA data, we show the multiple-muon rate as a function of the month of year in Fig. 5. That distribution is more sinusoidal than the rate as a function of time, as had been observed previously [17]. We perform the fit to the data in Fig. 5 and obtain $V_0 = 0.0 \pm 0.1$ %, $V = 4.1 \pm 0.2$ %, and ϕ = -0.43 $\pm$ 0.05 radians. The uncertainty is only that from the fit. This value of the phase corresponds to a maximum multiple-muon rate near 25 January and a minimum near 26 July. In all subsequent fits we set ϕ = -0.43 radians. The value of V_0 in every fit is consistent with zero.

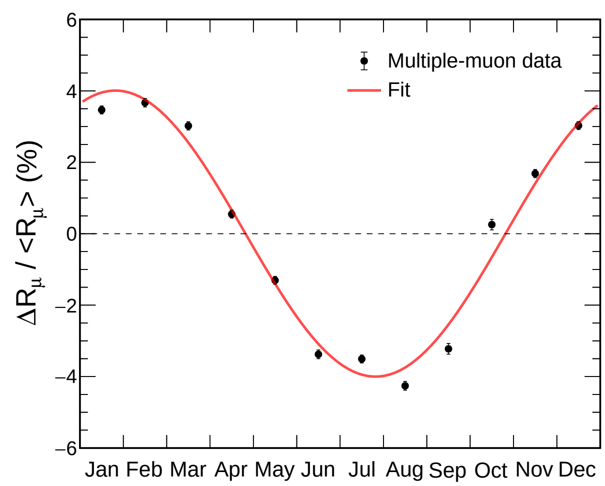

FIG. 5: Percentage rate variation of multiple muons in the NOvA ND as a function of month of year.

IV. STUDIES OF MULTIPLE-MUON OBSERVABLES IN THE NOVA ND

The minimum muon energy needed to reach the NOvA ND through the overburden depends on the zenith angle (θ_{zen}) and is approximately proportional to $\sec\theta_{zen}$. The highest energy muons come from the highest energy primary cosmic rays. Since the cosmic ray energy spectrum is a steeply falling function, a test of the seasonal variation as a function of zenith angle θ_{zen} can be used to look for an energy dependence.

The zenith angle distribution for each track in a multiple-muon event is shown in Fig. 6. The distribution is divided into nine equal data sets which were used to calculate the Rayleigh Power, α_T, and the amplitude V of the cosine fit. Those values for the nine regions are shown in Table I. There do not appear to be any differences between the seasonal variation of multiple-muons at low and high zenith angles.

In the MINOS Far Detector, a difference in the seasonal variation of multiple-muon events was seen as a function of separation distance between the muons [17]. In the smaller MINOS Near Detector the same variation was not seen. Since the typical transverse momentum (p_t) for a hadron in a hadronic interaction is 300 MeV/c,

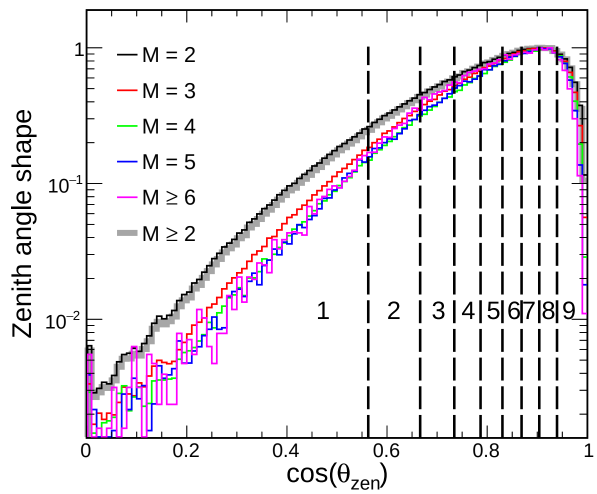

FIG. 6: Zenith angle distribution for each track in a multiple-muon event in the NOvA ND. Multiplicity distributions are normalized to have the maximum equal to 1 (one). The regions marked 1-9 have equal statistics.

Sample	$\cos\theta_{zen}$	P_R	α_T $\pm$ 0.1	V (%) $\pm$ 0.1	Tracks
1	$<$ 0.562	1475	-3.6	3.8	1,960,354
2	0.562-0.666	1624	-3.8	4.0	1,960,477
3	0.666-0.734	1732	-3.8	4.0	1,960,777
4	0.734-0.787	1778	-3.7	4.0	1,960,676
5	0.787-0.830	1715	-3.5	3.8	1,960,327
6	0.830-0.869	1807	-3.9	4.0	1,960,581
7	0.869-0.904	1667	-3.5	3.7	1,960,739
8	0.904-0.939	1562	-3.8	3.8	1,961,248
9	$>$ 0.939	1563	-4.2	4.2	1,957,395

TABLE I: Zenith angles are calculated for each track in a multiple-muon event. Measurements of the seasonal variation are shown for nine regions of $\cos\theta_{zen}$. The uncertainties on α_T and V are from the fit.

the distance between muons in the detector may decrease with increasing primary and muon energies. Multiple scattering in the overburden also affects this distance, but multiple scattering is smaller for larger muon energies. The track separation in NOvA is calculated by taking the perpendicular distance between every pair of tracks in a multiple-muon event

$$\Delta L = \cos\bar{\theta}_{zen} \times \sqrt{(\Delta X)^2 + (\Delta Z)^2}, \tag{4}$$

where X and Z are the horizontal detector coordinates of each track at the top of the detector and $\bar{\theta}_{zen}$ is the average zenith angle of the two tracks.

The square of the track separation ΔL is shown in Fig. 7. Nine equal-statistics regions (A...I) of track separation are defined with limits found in Table II. While the first and last bins show larger values of P_R, α_T and V, there does not appear to be any trend showing a difference between the seasonal variation of multiple-muons at large and small separation.

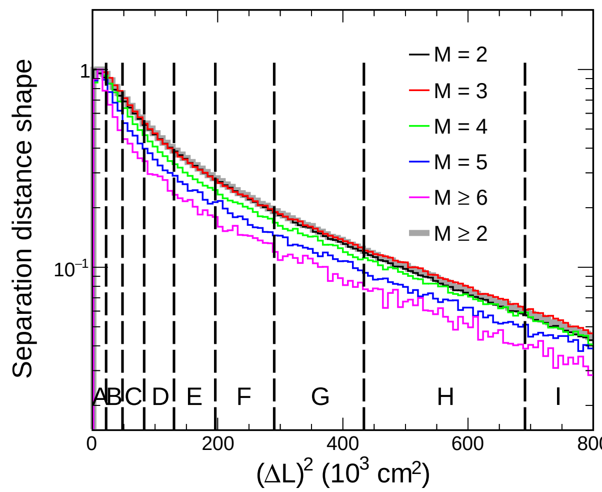

FIG. 7: Square of the separation ΔL between each track in each muon pair in a multiple-muon event in the NOvA ND. Multiplicity distributions are normalized to have the maximum equal to 1 (one). The regions marked A to I have equal statistics.

Sample	$(\Delta L)^2$ (10^3 cm^2)	P_R	α_T $\pm$ 0.1	V (%) $\pm$ 0.1	Pairs
A	$<$ 21.775	1861	-6.2	5.5	1,153,484
B	21.775-47.925	1477	-4.2	4.4	1,153,382
C	47.925-82.550	1439	-4.0	4.2	1,152,928
D	82.550-130.200	1485	-3.7	4.1	1,152,548
E	130.200-196.200	1461	-4.0	4.0	1,152,448
F	196.200-290.350	1406	-3.8	4.0	1,152,440
G	290.350-433.625	1490	-3.9	4.2	1,152,501
H	433.625-691.000	1501	-4.4	4.5	1,152,427
I	$>$ 691.000	1883	-5.3	5.2	1,149,599

TABLE II: Track separation squared for each pair of multiple-muon tracks, divided into nine regions of equal statistics, A...I. The uncertainties on α_T and V are from the fit.

The angle between tracks in a multiple-muon event is also related to the original muon energies. For this we compute

$$\theta_{UW} = \arccos\left(\frac{\vec{U}\cdot\vec{W}}{|\vec{U}||\vec{W}|}\right), \tag{5}$$

where $\vec{U}$ and $\vec{W}$ are vectors representing the directions of each pair of tracks in every multiplicity event. Track angles may diverge due to p_t in the first interaction, different locations for vertices in further interactions, multiple scattering, and magnetic bending. All of these effects are expected to be smaller for muons from higher energy primary cosmic rays. The angular resolution, which is a function of track length in the detector, affects this measurement. From a MC simulation of parallel tracks in the detector, the angular resolution for tracks which enter the top and exit the bottom is 1.6°. The distribution for the angle between all track pairs is shown in Fig. 8.

The track angle data were divided into nine equal samples (α...ι). The seasonal parameters for these nine regions of angular separation are shown in Table III. There is a possible reduction in the seasonal effect in the largest angle (ι) bin. We estimate a background of 600 two-muon events in two years from a coincidence of two random single-muon events within 100 ns, most of which will be in the ι region $\theta_{UW} > 15.55°$. This background causes a negligible systematic uncertainty to our fits. Another background which might contribute to the ι bin is hadronic interactions just above the detector.

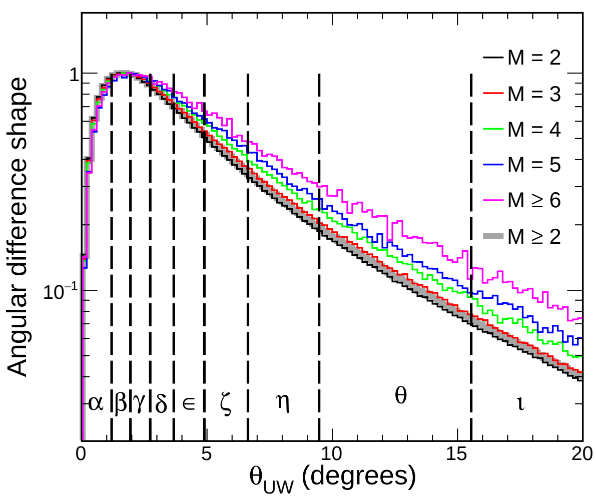

FIG. 8: Angle between each track in each muon pair in a multiple-muon event in the NOvA ND. Multiplicity distributions are normalized to have the maximum equal to 1 (one). The regions marked α to ι have equal statistics.

The muon multiplicity for multiple-muon events is a strong function of the primary cosmic ray energy. However, whatever dynamics are controlling the seasonality of multiple-muon events could be compounded as the multiplicity increases.

Since the statistics for each multiplicity are quite different, the Rayleigh power is not calculated. Also, α_T is not used since T_{eff} is multiplicity dependent in an unknown way. The amplitude fit for each multiplicity is shown in Table IV. The results of fitting the data to a cosine function for each multiplicity are shown in Fig. 9. A clear trend toward larger effects is seen as the multiplicity grows. The amplitude is shown as a function of multiplicity in Fig. 10.

Sample	θ_{UW} (degrees)	P_R	α_T	$V \pm 0.1$ (%)	Pairs
α	< 1.19	644	-4.2 ± 0.1	4.6	1,206,534
β	1.19-1.95	566	-4.0 ± 0.1	4.3	1,206,007
γ	1.95-2.74	607	-4.2 ± 0.1	4.4	1,207,553
δ	2.74-3.68	571	-4.1 ± 0.1	4.4	1,206,531
ε	3.68-4.90	582	-4.3 ± 0.1	4.4	1,206,217
ζ	4.90-6.64	541	-4.0 ± 0.1	4.3	1,206,216
η	6.64-9.48	590	-4.2 ± 0.1	4.5	1,206,275
θ	9.48-15.55	593	-4.4 ± 0.1	4.6	1,206,196
ι	> 15.55	332	-3.6 ± 0.2	3.5	1,200,193

TABLE III: Measurements of the seasonal variation for nine regions of angular separation of each muon pair in a multiple-muon event in the NOvA ND.

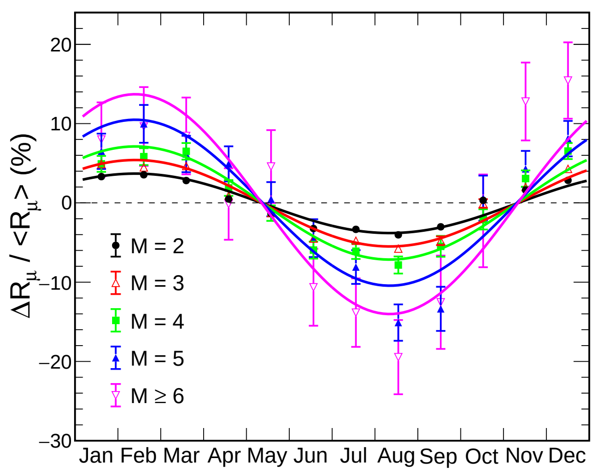

FIG. 9: Multiple-muon rate variation in the NOvA ND as a function of month of year, shown for each multiplicity. A cosine fit for each data sample is also shown, representing an increase in the size of the seasonal effect for larger multiplicities. In each fit, the phase ϕ is fixed to the value from the global fit.

V. SYSTEMATIC UNCERTAINTIES

Our conclusions involve the presence of a seasonal effect with a maximum in the winter which grows with multiplicity, and the absence of a noticeable trend in the size of that effect for three other variables. While there is no parameter for which a systematic uncertainty is appropriate, we must be confident that no systematic effect could create or mask the observed results. The Rayleigh power gives a measure of the statistical power of a pe-

Multiplicity	$V(\%)$	
2	3.81	$\pm$ 0.05
3	5.5	$\pm$ 0.2
4	7.1	$\pm$ 0.4
5	10.0	$\pm$ 0.9
≥ 6	14	$\pm$ 2
≥ 2	4.1	$\pm$ 0.2

TABLE IV: Amplitude as a function of multiplicity.

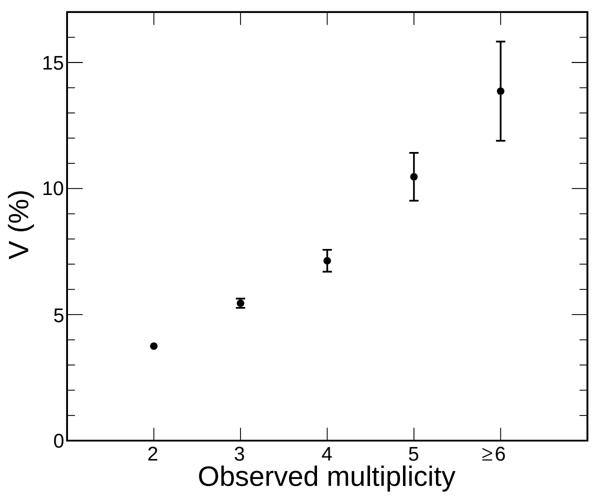

FIG. 10: Fitted amplitudes (%) to a cosine fit of the seasonal variation for each observed multiplicity in the NOvA ND.

riodic signal. For every sample studied, the Rayleigh power suggests the presence of a seasonal effect with a truly negligible chance probability.

The fits to α_T, which depends on temperature data, and the amplitudes V of the cosine fit, which do not depend on any temperature data, give qualitative measurements of the size of the seasonal variation which agree. The individual temperatures from ECMWF used to calculate T_{eff} have a systematic uncertainty of ± 0.31 K [12]. Based on the variation in temperature over the longitudinal area contributing to observed muon production, a systematic uncertainty on T_{eff} of ± 0.1 K was determined [26]. MINOS measured α_T for single muons at this location to be $+0.428 \pm 0.003(\text{stat}) \pm 0.059(\text{syst})$ [13]. The positive value indicates a summer maximum. We calculated α_T for single muons in NOvA and similarly found a summer maximum using daily and weekly time bins, and due to the lack of consistency in the value of α_T we assign a systematic uncertainty of $\pm$ 0.4, which corresponds to an uncertainty on the amplitude of $\pm 0.8\%$. This number provides a maximum correlated systematic uncertainty for α_T for multiple muons and includes all potential effects from temperature measurements and hardware or reconstruction issues which might be seasonally time dependent. Every measurement of α_T in Tables I, II, and III was negative with an absolute value at least 8 times this systematic uncertainty, indicating an unambiguous winter maximum. In the calculation of T_{eff}, the weighting of the atmospheric temperature versus altitude was done for the calculated location of single-muon and not multiple-muon production. The values of α_T in this analysis should be interpreted as a parameter indicating the size and sign of the seasonal effect, and not strictly the correlation coefficient between rate and an appropriately calculated T_{eff}.

The deadtime of the activity trigger used to acquire the cosmic ray data is slightly higher in the winter than the summer at the sub-percent level, due to the NuMI beam schedule. This deadtime difference based on our monitoring could affect the value of V by at most 0.5% and has not been corrected. This effect would be included in the $\pm 0.8\%$ uncertainty from the single-muon α_T inconsistency and could be the major contributor to it.

While the average temperature per month does not strictly follow a cosine curve, and hence its effect on seasonal variations would not either, the data in Figs. 5 and 9 follow a cosine function well enough for a fit to the amplitude of a cosine function to give a reasonable measure of the size of the seasonal variation. In order to evaluate the effect of the assumed shape of the distribution on the amplitude of the fit, a new fit was made by choosing a correlated systematic uncertainty on the rate such that $\chi^2/\text{dof} = 1$. That new fit to the data in Fig. 5 gave $V = 3.9 \pm 0.4$. We interpret 0.4 as a potential deviation in the value of V for the fact that true seasonal variations in our data do not follow a cosine. All values of V in Tables I, II, and III are at least 8 times this deviation.

The reconstruction program that we used did not reconstruct all triggered muons, particularly short and steep tracks. The inefficiency was not negligible. Visual inspection and MC studies showed that all reconstructed events were pure in the sense that there were at least the identified number of throughgoing muons in each event. For example, a reconstructed 3-muon event could possibly have 4 or more throughgoing tracks, but not 0, 1 or 2. This reconstruction issue could decrease the apparent size of that dependence but could not create a spurious dependence. The known steep falloff in the true multiplicity distribution [31] implies this uncorrected multiplicity distribution does not change our conclusion that the seasonal effect grows with multiplicity. The conclusion in the paper, that there is a multiplicity dependence as indicated in Fig. 10, is robust.

We have not identified any systematic uncertainty which depends strongly on spatial separation, angular separation, or zenith angle. The systematic uncertainties involving deadtime and temperature cancel to first order when dividing the data into bins of these observables and do not mask the lack of trends in Tables I, II, and III.

VI. SUMMARY AND DISCUSSION

The NOvA ND data show that the rate of multiple muons seen at a depth of 225 mwe underground is anticorrelated with the temperature of the atmosphere. That is, the rate increases in the winter and decreases in the summer. This anticorrelation between temperature and rate was also observed previously [17].

In this analysis we used several proxies for the initial muon and primary cosmic ray energies to see if the effect was related to the particle initial energy; there is no indication that is the case. However, we observe the effect grows from 4% to 14% with increasing muon multiplicity. This is a new observation, which may allow one to clarify further the physics origin of the observed puzzling behavior. The quantitative nature of this anticorrelation is not understood. This result is consistent with the suggestion from the previous analysis in which the effect is attributed to multiple muons coming from those π's which are more likely to interact than decay in the winter [17]. Thus the single-muon rate is higher in the summer and the multiple-muon rate is higher in the winter.

The mean surface muon energy for muons reaching a depth of 225 mwe is below the critical energy for both π's and K's, so that more secondary hadrons are decaying before they interact in the upper atmosphere. For detectors at depths of 2000 mwe or more, the mean muon energy is above the critical energy for π's and comparable to the critical energy for K's. The observed effect at 2000 mwe is more complicated than just a dependence on the π and K critical energies and so further studies should be done at those depths. The results from the NOvA ND presented in this paper will be important inputs to future simulation and study of this effect.

VII. ACKNOWLEDGMENTS

This document was prepared by the NOvA collaboration using the resources of the Fermi National Accelerator Laboratory (Fermilab), a U.S. Department of Energy, Office of Science, HEP User Facility. Fermilab is managed by Fermi Research Alliance, LLC (FRA), acting under Contract No. DE-AC02-07CH11359. This work was supported by the U.S. Department of Energy; the U.S. National Science Foundation; the Department of Science and Technology, India; the European Research Council; the MSMT CR, GA UK, Czech Republic; the RAS, RFBR, RMES, RSF, and BASIS Foundation, Russia; CNPq and FAPEG, Brazil; STFC, and the Royal Society, United Kingdom; and the state and University of Minnesota. We are grateful for the contributions of the staffs of the University of Minnesota at the Ash River Laboratory and of Fermilab.

---

[1] P. Barrett *et al.*, Rev. Mod. Phys. **24**, 133 (1952).
[2] N. Sherman, Phys. Rev. **93**, 208 (1954).
[3] G. C. Castagnoli and M. A. Dodero, Nuovo Cim. B **51**, 525 (1967).
[4] A. Fenton, R. Jacklyn and R. Taylor, Nuovo Cim. B **22**, 285 (1961).
[5] Y. Andreyev *et al.*, (Baksan Collaboration), Proceedings of the 20th ICRC, vol. 4, pp. 270 (1987).
[6] M. Ambrosio *et al.*, (MACRO Collaboration), Astropart. Phys. **7**, 109 (1997).
[7] A. Bouchta (AMANDA Collaboration), Proceedings of the 26th ICRC, vol. 2, pp. 108-111 (1999).
[8] G. Bellini *et al.*(Borexino Collaboration), JCAP05 015 (2012), hep-ex/1202.6403.
[9] M. Selvi (LVD Collaboration), Proceedings of the 31st ICRC (2009).
[10] P. Desiati *et al.*, (IceCube Collaboration), Proceedings of the 32nd ICRC (2011), astro-ph/1111.2735.
[11] S. Osprey *et al.*, (MINOS Collaboration), Geophys. Res. Lett. **36**, L05809 (2009).
[12] P. Adamson *et al.*, (MINOS Collaboration), Phys. Rev. D **81**, 012001 (2010), hep-ex/0909.4012.
[13] P. Adamson *et al.*, (MINOS Collaboration), Phys. Rev. D **90**, 012010 (2014).
[14] T. Abrahao *et al.*, (Double Chooz Collaboration), JCAP02 017 (2017).
[15] F. P. An *et al.*, (Daya Bay Collaboration), JCAP01 001 (2018).
[16] R. P. Feynman, Phys. Rev. Lett. **23**, 1415 (1969).
[17] P. Adamson *et al.*, (MINOS Collaboration), Phys. Rev. D **91**, 112006 (2015).
[18] K. P. Arunbabu *et al.*, Astropart. Phys. **94**, 22 (2017).
[19] R. P. Kokoulin et al, (DECOR Collaboration), Proceedings of the 34th ICRC (2015), N. V. Talkacheva *et al.*, Bulletin of the Russian Academy of Sciences, Physics **75** 377 (2011).
[20] D.S. Ayres *et al.*, NOvA Technical Design Report, FERMILAB-DESIGN-2007-01.
[21] P. Adamson *et al.*, Nucl. Inst. and Meth. A **806**, 279 (2016); NuMI Technical Design Handbook, FERMILAB-PUB-15-253-AD-FESS-ND.
[22] R. L. Talaga *et al.*, Nucl. Inst. and Methods, A **861**, 77-89 (2017).
[23] S. Mufson et al., Nucl. Instrum. Meth. A 799, 1 (2015).
[24] L. A. F. Fernandes and M. M. Oliveira, Pattern Recognition **41**, 299 (2008).
[25] C. Hagmann, D. Lange and D. Wright, IEEE Nuclear Science Symposium conference record. Nuclear Science Symposium 2:1143 - 1146 October-November 2007.
[26] S. C. Tognini, Ph.D. thesis, Federal University of Goias, (2018) https://ccd.fnal.gov/techpubs/fermilab-reports-thesis.html.
[27] D. P. Dee *et al.*, Quart. JR Meteorol. Soc. **137**, Issue 656, 553, (2011). Information and data are available at https://www.ecmwf.int/.
[28] A. Norman, E. Niner and A. Habig, Journal of Physics: Conference Series **664** 082040, 2015.
[29] E. Grashorn *et al.*, Astropart. Phys. **33** 140 (2010).

[30] W. H. Press and G. B. Rybicki, AstroPhys. Jour. **338** 277 (1989).

[31] S. M. Kasahara *et al.*, Phys. Rev. D **55** 5282 (1997).